

# Demands and distribution of hysteretic energy in steel self-centering MRFs

A. López Barraza<sup>\*1</sup>, S. E. Ruiz<sup>1,a</sup>, A. Reyes Salazar<sup>2,b</sup>, E. Bojórquez<sup>2,c</sup>

<sup>1</sup>*Instituto de Ingeniería, Universidad Nacional Autónoma de México, México City, México*

<sup>2</sup>*Facultad de Ingeniería, Universidad Autónoma de Sinaloa, Culiacán, Sinaloa, México*

**Abstract.** Post-tensioned (PT) steel moment resisting frames (MRFs) with semi-rigid connection (SRC) are a viable alternative to be used for earthquake resistant steel buildings. Their capacity of self-centering and ability to dissipate energy concentrating the damage on elements easily replaceable make them attractive for structures in seismic prone areas. Moreover, steel MRFs with PT connections can be used for the control of hysteretic energy demands and to reduce the maximum inter-story drift ( $\gamma$ ). In this study the seismic behavior of steel MRFs with PT connections is estimated by incremental nonlinear dynamic analysis in terms of dissipated hysteretic energy ( $E_H$ ) demands. For this aim, five PT steel MRFs are subjected to 30 long duration earthquake ground motions recorded on soft soil sites of Mexico City. To better assess the energy dissipated in the frames with PT connections, a new expression is proposed for the hysteretic behavior of SRC validated by experimental tests. The performance was estimated not only using the global  $E_H$  demands in the steel frames; further, the distribution and demands of hysteretic energy in beams, columns and connections were assessed at different demands of  $\gamma$ . The results show that  $E_H$  varies with  $\gamma$ , and that most of  $E_H$  is dissipated by the connections. It is observed in all the cases a log-normal distribution of  $E_H$  through the building height. The largest demand of  $E_H$  occurs between 0.25 and 0.5 of the height. Finally, an equation is proposed to calculate the distribution of  $E_H$  in terms of the normalized height of the stories ( $h/H$ ) and the inter-story drift.

**Keyword:** steel frames; self-centering; post-tensioned connections; hysteretic energy; inter-story drift

## 1. Introduction

Post-tensioned steel moment resisting frames are structural systems proposed in recent years as an appropriate alternative to welded connections of moment resisting frames in seismic zones (Ricles *et al.* 2001, 2002, 2010, Christopoulos *et al.* 2002a, 2002b, 2003, Garlock *et al.* 2005, 2007, 2008, Kim *et al.* 2009, Chung *et al.* 2009, Wolski *et al.* 2009, Tong *et al.* 2011). They are designed to prevent brittle fractures in the area of the nodes of steel frames, which can cause severe reduction in their ductility capacity, as occurred in many cases during the 1994 Northridge and the 1995 Kobe earthquakes. Under the action of an intense earthquake motion, beams and columns remain essentially elastic concentrating the damage on the energy dissipating elements, which can be easily replaced at low cost. Moreover, they provide capacity of energy dissipation and self-centering reducing the residual displacements. It is important to consider the residual displacements on the buildings after a seismic event, as they may require heavy spending on repairs or the total demolition in the case of excessive structural damage. Recent studies of steel frames have shown that the maximum and residual drifts of PT steel

\*Corresponding author. Ph.D. Student, E-mail: [alopezb@uas.edu.mx](mailto:alopezb@uas.edu.mx)

<sup>a</sup>Professor, E-mail: [sruizg@iingen.unam.mx](mailto:sruizg@iingen.unam.mx)

<sup>b</sup>Professor, E-mail: [reyes@uas.edu.mx](mailto:reyes@uas.edu.mx)

<sup>c</sup>Professor, E-mail: [eden@uas.edu.mx](mailto:eden@uas.edu.mx)

MRFs are up to 50% of those of equivalent frames with welded connections (Lopez-Barraza *et al.* 2012).

Although the maximum inter-story drift is one of the main parameters used in seismic design codes to guarantee a satisfactory seismic performance of structures, this parameter does not explicitly consider the effect of cumulative structural damage due to plastic deformation, which can be accounted by means of the dissipated hysteretic energy. The estimation of hysteretic energy demands is especially important for structures subjected to long duration earthquake ground motions such as those occurring in the Valley of Mexico (Terán-Gilmore 2001, Bojórquez and Ruiz 2004). Some researchers have proposed seismic design methodologies that consider the cumulative effect of plastic deformation demands and the effect of the duration on the structural response (Akiyama 1985, Cosenza and Manfredi 1996, Terán-Gilmore 1996, Hancock and Bommer 2006). One way to explicitly consider the accumulated damage is through concepts of seismic energy. Methods based on energy concepts are oriented to provide the system with an energy capacity greater than or equal to the energy demanded by the earthquakes (Uang and Bertero 1990). Seismic design methodologies exclusively based on dissipated hysteretic energy have been recently developed (Akbas *et al.* 2001, Choi and Shen 2001, Choi and Kim 2006, Bojórquez *et al.* 2008, Choi and Kim 2009); and damage indicators based only on  $E_H$  were proposed (Terán and Jirsa 2005, Bojórquez *et al.* 2010), since  $E_H$  is closely related to structural damage. A very important aspect of the hysteretic energy, when it is used as a structural performance parameter is its distribution through the height of the building. Several researchers have proposed some alternatives regarding the way of  $E_H$  is distributed in steel structures but they are exclusively applied to MRFs. For example, Akbas *et al.* (2001) proposed to use a linear distribution of hysteretic energy along the height. Studies conducted by Bojórquez *et al.* (2008) in steel frames with rigid connections, suggested that when the energy dissipated by plastic behavior is concentrated in the beams of a structural framework, a log-normal function represents the form in which the energy is dissipated through the height.

In this paper, the seismic behavior of PT steel MRFs is studied in terms of dissipated energy. The frames are designed so that the demands of  $E_H$  focus on the dissipator elements placed in the connections in the case angles as will be detailed below, while beams and columns remain essentially elastic. However, the demands of  $E_H$  in columns and beams are also estimated. Equations are proposed to calculate the distribution factors for hysteretic energy through height ( $F_{EH}$ ). They depend on the maximum inter-story drift demands. In order to calculate  $E_H$  in the post-tensioned semi-rigid connections, new equations that accurately represent the hysteretic cycles are proposed. These equations were validated by experimental tests carried out by the authors and other developed by Garlock (2005). They are continuous functions that depend only on a few parameters in order to facilitate their use. Knowing the hysteretic energy distribution through the height is an important aspect to propose seismic design procedures of buildings (Bojórquez *et al.* 2008).

## 2. Structural models

### 2.1 Self-centering steel frames

The hysteretic energy distribution along the height is characterized by a factor which is obtained from the analysis of five post-tensioned steel frames. The semi-rigid connection is achieved by connecting the flanges of tension and compression beam to the column by bolted angles (TS, top and seat connection); these angles dissipate energy through hysteretic behavior in the connection. To design the five steel MRFs with PT connections, a procedure proposed by Garlock *et al.* (2007) is used where beams and columns of the frame are designed by considering the connections as rigid. Later, connections and post-tensioning elements are designed to meet service and resistance requirements. The frames were designed according to the seismic regulations of the Mexican City Building Code (MCBC 2004). The structures, which are used as office occupancy buildings, are supposed to be located on the soft soils of Mexico City. They are 4-, 6-, 8-, 10- and 14- story buildings having 3 bays, hereafter identified

as F4PT, F6PT, F8PT, F10PT and F14PT, respectively. Their fundamental periods ( $T_1$ ) are 0.89, 1.03, 1.25, 1.37 and 2.10s respectively. The dimensions of the structural frames are given in Fig. 1. The beams and columns are W sections of A36 steel. A bilinear model with 3% of post-yield stiffness and 3% of critical damping is considered for the analyses. In the design of the connections steel grade 50 was used for angles, and steel A490 for the screws, which have a diameter of 25 mm. The length of the angles was taken equal to the width of the flange of the beams ( $b_f$ ). Different angle sizes were tested. In the end, 152x16 mm angles were used in the connection of F4PT model while 152x13 angles were used in the remaining frames. To prevent collapse and local buckling of the flanges, reinforcing plates with a thickness of 25 mm, width equal to  $b_f$  and a length 1000 mm were placed by welding at the ends of the beams. Post-tensioned cables consist of seven wires with an area of 150 mm<sup>2</sup> and withstanding a load of 279 kN; they are parallel to the axis of the beam passing through the interior columns and fixed to the outer face of the columns at the ends of the frame. Fig. 2 shows a typical assembly in which the tensioned elements and the energy-dissipating elements for the case of screwed angles can be identify.

## 2.2 Hysteretic model for post-tensioned connections

The seismic behavior of post-tensioned connections is usually expressed in terms of  $M-\theta_r$  (moment-relative rotations) curves. Experimental tests with assemblies of beams and columns connected by post-tensioned screwed angles show that the  $M-\theta_r$  curves present a nonlinear behavior resembling a flag (Ricles *et al.* 2002, Garlock *et al.* 2005, Pirmoz and Danesh 2009, Kim *et al.* 2010), which characterizes the non-linearity, the self-centering capability and the capacity of energy dissipation. Experimental tests with isolated angles, subjected to cyclic and monotonic loads conducted by Shen and Astaneh-Asl (1999) showed a stable cyclic response and good capability of hysteretic energy dissipation. Ultimate strength exceeded 3 times the yield strength and ductility reached values between 8 and 10. The above observations were confirmed in a series of experiments with angles developed by the authors. 152x13 and 152x10 angles with gages ( $g_a$ ) of 80, 90, 100 and 108 mm were tested for monotonic and cyclic loading for ductility demands of 3, 6, 12 and 18. It was observed that the number of cycles to failure depends on the ductility demand and that there is a specific ductility demand value for which the hysteretic energy dissipation capacity of the angles is maximum; for the cases under consideration this ductility demand is 6. Fig. 3 shows the results for the particular case of 152x10 angles with  $g_a = 100$  mm. It can be seen that the monotonic curve is the envelope of the curves of the hysteretic cycles. Moreover, for a given value of ductility demand, the hysteresis loops present a stable behavior.

Fig. 4 shows the main elements that are part of a post-tensioned connection including their deformation. The strength and stiffness for bending of the post-tensioned connection come from the contribution of the angles of the TS connection and those provided by the post-tensioned cables. Wires and angles work as springs in parallel. Post-tensioned wires exhibit linear behavior, while connecting angles behave non-linearly since the beginning of the deformation. There are numerous experimental and analytical studies of TS connections with bolted angles to model the angle participation. Bi-linear, polynomial and exponential functions have been proposed to characterize the  $M-\theta_r$  curve (Richard and Abbott 1975, El-Salti 1992). In order to numerically evaluate the  $E_H$  dissipated in a connection with acceptable precision, it is very important to have equations that represent with good approximation the  $M-\theta_r$  curve for loading and unloading cycles of semi-rigid post-tensioned connections. Two exponential functions are presented in this paper. The first function, given by Eq. (1), corresponds to the initial loading cycle; two types of variables are observed: 1) variables depending only on geometric and physical properties of angles, such as initial ( $k$ ) and post-yield ( $k_p$ ) stiffness, the reference moment ( $M_o$ ) and  $N$  that defines the curvature in the transition between the linear and plastic behavior and 2) variables depending on the number and type of tendons such as the rigidity of the post-tensioned tendons ( $k_{\theta S}$ ) and, the bending moment associated to the opening of the connection (named decompression moment,  $M_d$ ) which is a function of the resulting initial tension in the tendons. The second function, given by Eq. (2), defines the unloading and

reloading process in the connection;  $M_a$  and  $\theta_a$  are the maximum values reached in each cycle, the parameter  $\varphi$  defines the magnitude of the closing moment of the connection ( $M_c$ ), which must be greater than zero in order to insure complete closure of the connection after getting complete unloading; moreover, this parameter largely defines the  $E_H$  dissipation capacity of the connection (enclosed area). The interpretation of some of the parameters described above is shown in Fig. 5a.

The accuracy of the proposed equations is compared with experimental results. Fig. 5a shows several complete cycles of loading and unloading obtained from Eqs. (1) and (2), together with experimental results obtained in this study. Equivalent graphs are shown in Fig. 5b together with experimental results of the 36s-20-P specimen published by Garlock *et al.* (2005).

$$M = M_d + \frac{(k - k_p)\theta_r}{\left[1 + \left|\frac{(k - k_p)\theta_r}{M_o}\right|^N\right]^{\frac{1}{N}}} + (k_p + k_{\theta S})\theta_r \quad (1)$$

$$M = M_a - \frac{(k - k_p)(\theta_a - \theta_r)}{\left[1 + \left|\frac{(k - k_p)(\theta_a - \theta_r)}{\varphi M_o}\right|^N\right]^{\frac{1}{N}}} - (k_p + k_{\theta S})(\theta_a - \theta_r) \quad (2)$$

### 3. Seismic ground motions

The structural models described above were subjected to 30 narrow-band long duration ground motions. The narrow-band earthquakes particularly affect structures within a short interval of periods (especially those suffering of softening or with structural periods close to the period of the soil). In fact, these records demand large amounts of energy to structures compared to broad-band records (Terán and Jirsa 2007). The ground motions were recorded in sites where the period of the soil was close to two seconds and the more severe damage on structures was observed, during the Mexico City Earthquake of September 19, 1985. Table 1 shows the magnitude, acceleration, velocity and duration of each of the seismic records considered. Note that the duration was computed according with Trifunac and Brady (1975).

### 4. Hysteretic energy distribution in the frames

One of the requirements in the design of steel MRFs with PT connections is to concentrate plastic deformations in the angles of the connections while beams and columns remain essentially elastic under strong earthquakes, in such a way that the angles can be easily replaced in the case of excessive structural damage. To determine the  $E_H$ , incremental dynamic analysis is performed for each frame subjected to a set of 30 seismic records scaled at different values of seismic intensity in terms of spectral acceleration at fundamental period of vibration of the structure  $Sa(T_1)$ . The seismic intensity varies from 0.1g to 3.0g with increments of 0.1g. RUAUMOKO program (Carr 2011) was used for non-linear, step-by-step dynamic analysis. To show how the demands of  $\gamma$  and  $E_H$  are distributed, the F10PT model is subjected to the earthquake ground motion 1 scaled to  $Sa(T_1)=1.3g$ , the maximum inter-story drift demands are shown in Fig. 6, the maximum value is 0.030 and occurs at 4th floor. Fig. 7a shows the  $E_H$  dissipated by the structural elements; the connections dissipate 57.8% and the columns 42.2%.

The beams do not dissipate energy, implying that there is no plastic deformation on them. Fig. 7b shows the  $E_H$  dissipated by the columns for each inter-story; it is observed that the base columns are the only ones that dissipate energy, the reason for this is that the supports of these columns are fixed, resulting in the formation of plastic hinges in that location even for moderate seismic demands. The connections dissipate energy on every floor, being larger on Floors 3, 4 and 5, as shown in Fig. 7c. A similar distribution is observed for  $\gamma$  (Fig. 6) and for  $E_H$  (Fig. 7c).

The  $E_H$  is now estimated for a target value of  $\gamma$ . For each PT frame model, subjected to all earthquakes, scaled to different levels of seismic intensity, the values of  $\gamma$  and the corresponding value of  $Sa(T_1)$  are plotted and the median of maximum inter-story drift ( $\bar{\gamma}$ ) is calculated. This curve gives the required value of  $Sa(T_1)$  to produce the target value of median maximum inter-story drift; that is, the relationship between seismic intensity and the median value of the maximum inter-story drift is obtained. Fig. 8 shows the results for the F10PT model, discrete values of  $\gamma$  are obtained for the thirty earthquakes scaled to  $Sa(T_1)$  varying from 0.1 to 3.0g. The solid line represents  $\bar{\gamma}$ , from which it is possible to read the values of  $Sa(T_1)$  for specific values of  $\bar{\gamma}$ . Table 2 shows the magnitudes of  $Sa(T_1)$  for four values of  $\bar{\gamma}$  for all models; it can be seen that for a given  $\bar{\gamma}$ , the seismic intensity magnitude increases as the height of the building increases. Note that values of  $Sa(T_1)$  are not reported for the F14PT model for  $\bar{\gamma}=0.03$  and 0.05 because the probability of having values greater than 3g is small.

Table 3 contains the  $E_H$  dissipated by the columns, beams and connections corresponding to different demands of maximum drift. The results are presented for the average values of  $E_H$ , in percentage, demanded by the 30 earthquakes scaled to the same seismic intensity normalized with respect to the total  $E_H$ . The participation of the beams is very small, implying that the connections and the columns mostly dissipate the energy. It is observed that the participation of connections increases and the participation of the columns decreases as the number of levels increases.

Fig. 9 shows the average dissipated  $E_H$  in the F10PT model for a maximum inter-story drift demand of 0.03 (earthquakes escalated to  $Sa(T_1)=1.8g$ ). It is observed that 59.6% of the total  $E_H$  is dissipated by connections, 40.2% by columns and only 0.2% by beams. Fig. 10 shows how the demands of  $E_H$  are distributed in columns, beams and connections for each level. The total energy dissipated by the columns is concentrated in the first story, because the columns are fixed supports in the base, as previously explained. The distribution of  $E_H$  in the beams is negligible. The connections dissipate energy on every floor, being larger on Floors 3, 4 and 5 and smaller on Floors 9 and 10. In this case, a lognormal distribution of  $E_H$  through the height is appropriate. Similar results were observed for the other models, where it was also observed that the participation of the connections in dissipating hysteretic energy increases when the number of stories increases; this is expected since the number of connections increases while the number of columns that dissipate energy remain the same (at the base).

## 5. Hysteretic energy distribution factors ( $F_{EH}$ )

The distribution of hysteretic energy demands in the structures is an important aspect that needs to be considered in seismic design methodologies based on this parameter. Since  $\gamma$  is the parameter commonly used to achieve satisfactory seismic performance, it is desirable to have an expression for estimating hysteretic energy demands and its distribution along the height as a function of  $\gamma$ . In order to obtain the distribution of hysteretic energy through height, the structures were subjected to all the seismic records under consideration which are scaled until a specific value of the median maximum inter-story drift is obtained. The procedure for estimating the  $F_{EH}$  is as follows:

Step 1. Incremental dynamic analysis of the steel frame is carried out using all the seismic records scaled to different levels of seismic intensity in terms of  $Sa(T_1)$ .

Step 2. The median maximum inter-story drift ( $\bar{\gamma}$ ) is plotted and the required value of  $Sa(T_1)$  that produces the target value of maximum inter-story drift is obtained.

Step 3. The hysteretic energy distribution is obtained for values of specific seismic intensity for each seismic record; then the average hysteretic energy on each floor is calculated.

Hysteretic energy distribution factors  $F_{EH}$  are obtained by dividing the average hysteretic energy of each floor and the average hysteretic energy of the floor undergoing the largest energy demand.

Fig. 11 shows the  $F_{EH}$  values for each floor at several levels of inter-story drift demands of the F6PT and F10PT models;  $h/H$  is the height of each floor normalized by the total height of the structure ( $H$ ) relative to the ground level. It is observed that the distribution of  $E_H$  through height is essentially log-normal for different levels of inter-story drift demand, the same occurs for the F4PT, F8PT and F14PT models. It is observed also that an increment in the inter-story drift causes a greater participation of the upper floors in plastic energy dissipation.

## 6. Equation for the estimation of $F_{EH}$

From the results obtained from the analyses of the post-tensioned steel regular frames, it is observed for all cases that the distribution of dissipated hysteretic energy along the height can be represented in a reasonable manner by a log-normal distribution. Eq. (3) is proposed to estimate  $F_{EH}$  as a function of building height and the maximum demand of inter-story drift.

$$F_{EH} = \frac{1}{f_1\left(\frac{h}{H}\right)} \exp\left\{-\frac{1}{2} \left[ \frac{\ln\left(\frac{h}{H}\right) - \ln(f_2(\gamma))}{f_3(\gamma)} \right]^2\right\} \quad (3)$$

In equation 3, the parameters  $f_1(\gamma)$ ,  $f_2(\gamma)$  and  $f_3(\gamma)$  are a function of the maximum inter-story drift demand, and are obtained from regression analysis of  $F_{EH}$  calculated for all the frames analyzed and their respective levels of inter-story drift demand.

Eqs. (4), (5) and (6), obtained from regression analysis of  $F_{EH}$  for all the frames, define the parameters of Eq. (3).

$$f_1(\gamma) = 5.343\gamma + 2.433 \quad (4)$$

$$f_2(\gamma) = 1.380\gamma + 0.388 \quad (5)$$

$$f_3(\gamma) = 8.374\gamma + 3.316 \quad (6)$$

Eq. (3) is plotted with solid lines in Fig. 12, together with the discrete values of  $F_{EH}$  obtained for maximum drifts of 0.015, 0.020, 0.030 and 0.050 for all frames. It is observed that the number of levels or structural period of vibration of the frames does not affect the shape of the distribution of  $E_H$  through height; note also that the largest energy demands are obtained for  $0.25 \leq h/H \leq 0.5$ . Fig. 12 suggests that the calculated values of  $F_{EH}$  with the proposed equation can be obtained with good accuracy, although it is slightly overestimated for the upper floors. Table 5 shows the  $F_{EH}$  values calculated with Eq. (3) for different demands of inter-story drift; it can be seen that the peak demand of  $E_H$  is given for  $h/H = 0.3$  for all values of  $\gamma$ . It is also observed that the  $F_{EH}$  values increase at other levels of the frames as the values of  $\gamma$  increase. Eq. (3), together with the values given by Eqs. (4), (5) and (6), is fitted with good accuracy to the distribution of  $E_H$  obtained from the step-by-step nonlinear dynamic analysis, indicating that the expression can reasonably be used to estimate the energy distribution through the height of regular PT steel moment resisting frames.

## 7. Conclusions

The capacity of self-centering and ability to dissipate energy of post-tensioned moment resisting steel frames make them a viable alternative for steel buildings in earthquake zones. The concentrations of damage on elements, which can be easily replaceable, make them attractive for structures in seismic prone-areas. Because the maximum inter-story drift ( $\gamma$ ) is one of the main parameters used in seismic design codes to ensure a satisfactory seismic performance of structures, but this parameter does not explicitly contemplate the effect of accumulated structural damage caused by plastic deformation. In this paper, the seismic behavior of post-tensioned moment resisting steel frames is studied in terms of dissipated hysteretic energy, due to the ability of this parameter to incorporate cumulative damage. Five steel frames were subjected to 30 ground motion records of soft soil sites.

Firstly, an expression is proposed to estimate energy dissipated by hysteretic behavior of post-tensioned semi-rigid connections. The equation, which models the hysteretic cycles of this type of connections, exhibits an excellent accuracy when compared with experimental results.

The distribution and demands of hysteretic energy ( $E_H$ ) in beams, columns and connections were determined for different demands of  $\gamma$ . It is observed that  $E_H$  varies with  $\gamma$ , and that, except for the columns at the base,  $E_H$  is dissipated by plastic deformation of the angles in the connection; the other structural components remain elastic even for large demands of the inter-story drift. It is observed in all cases a log-normal distribution of  $E_H$  with height. The greatest demand of  $E_H$  occurs between 0.25 and 0.5 of height. The tallest buildings exhibit a smoother variation of  $E_H$  through height for all inter-story drift levels. This distribution does not depend on the fundamental periods of the models. In the case of the upper floors, the hysteretic energy demands tend to increase as the maximum inter-story drift increases. Based on these results, an equation is proposed to calculate the hysteretic energy distribution factors ( $F_{EH}$ ) in terms of the relative height of the stories ( $h/H$ ) and  $\gamma$ . The proposed equation can be used to accurately estimate the distribution of  $E_H$  demands in post-tensioned moment resisting steel frames.

## Acknowledgments

This study was supported by Secretaría de Educación Pública (PROMEP/103.5/10/5408), Universidad Nacional Autónoma de México (DGAPA-UNAM under project IN-107011), and by Universidad Autónoma de Sinaloa (under grant PROFAPI/2011/142). Any opinions, findings, conclusions, or recommendations expressed in this publication are those of the authors and do not necessarily reflect the views of the sponsors.

## References

- Akbas, B., Shen, J. and Hao, H. (2001). "Energy approach in performance-based design of steel moment resisting frames for basic safety objective", *The Structural Design of Tall Buildings*, **10**, 193-217.
- Akiyama, H. (1985). "Earthquake-Resistant Limit-State Design for Buildings", *University of Tokyo Press*, Tokyo.
- Arias, A. (1970), "A measure of earthquake intensity", *Seismic Design for Nuclear Power Plants*, Eds. Hansen, R.J., MIT Press, Cambridge, MA, 438-483.
- Bojórquez, E. and Ruiz, S. E. (2004). "Strength reduction factors for the valley of Mexico taking into account low cycle fatigue effects", *13<sup>o</sup> World Conference on Earthquake Engineering*, paper 516, Vancouver, Canada 2004 (CD-ROM).
- Bojórquez, E. and Rivera, J.L. (2008), "Effects of degrading models for ductility and dissipated hysteretic energy in uniform annual failure rate spectra", *The 14th World Conference on Earthquake Engineering*, Beijing, China .
- Bojórquez, E., Ruiz S. E. and Terán-Gilmore A. (2008). "Reliability-based evaluation of steel structures using energy concepts", *Engineering Structures*. **30**(6), 1745-1759.

- Bojórquez, E., Reyes-Salazar A., Terán-Gilmore A. and Ruiz S.E. (2010), "Energy-based damage index for steel structures", *Journal Steel and Composite Structures*, **10**(4), 343-360.
- Carr A. (2011) "RUAUMOKO" *Inelastic Dynamic Analysis Program*, University of Canterbury, Department of Civil Engineering.
- Choi, B. J. and Shen, J. H. (2001). "The establishing of performance level thresholds for steel moment-resisting frame using an energy approach", *Estruct. Design Tall Build*, **10**, 53-67.
- Choi, H. and Kim, J. (2006). "Energy-based seismic design of buckling-restrained braced frames using hysteretic energy spectrum", *Engineering Structures*, **28**, 304-311.
- Choi, H. and Kim, J. (2009). "Evaluation of seismic energy demand and its application on design of buckling-restrained braced frames", *Structural Engineering and Mechanics*, **31**, 93-112.
- Christopoulos, C., Filiatrault, A. and Uang, C.M. (2002a). "Self-centering post-tensioned energy dissipating (PTED) steel frames for seismic regions", University of California, Report No. SSRP-2002/06.
- Christopoulos, C. and Filiatrault, A. (2002b). "Seismic response of posttensioned energy dissipating moment resisting steel frames", Proceedings of the 12th European Conference on Earthquake Engineering, London, UK, paper No. 61.
- Christopoulos, C., Filiatrault, A., and Uang, C.-M. (2003). "Seismic demands on post-tensioned energy dissipating moment-resisting steel frames." *Proc., Steel Structures in Seismic Areas (STESSA)*, Naples, Italy.
- Chung, C. C., Tsai, K.C. and Yang, W.C. (2009). "Self-centering steel connection with steel bars and a discontinuous composite slab", *Earthquake Engng Struc. Dyn.*, **38**, 403-422.
- Cosenza E, Manfredi G. (1996), "Seismic design based on low cycle fatigue criteria ".XI World Conference on Earthquake Engineering (CD), paper 1141, Acapulco, México.
- El-Salti Maher Kh. (1992), "Design of Frames with Partially Restrained Connections" PhD dissertation, The University of Arizona
- Garlock, M, Ricles, J., and Sause, R. (2005) "Experimental Studies on Full-Scale Post Tensioned Steel Connections", *Journal of Structural Engineering*, ASCE, **131**(3), 438-448.
- Garlock, M, Sause, R. and Ricles, J., (2007). "Behavior and Design of Posttensioned Steel Frames System" *Journal of Structural Engineering*, ASCE, **133**(3), 389-399.
- Garlock, M, Sause, R. and Ricles, J., (2008). "Influence of design parameter on seismic response of post-tensioned steel MRF systems ", *Engineering Structures*, **30**, 1037-1047.
- Hancock, J., and J. J. Bommer, (2006). A state-of-knowledge review of the influence of strong-motion duration on structural damage, *Earthquake Spectra*, **22**, 827-845.
- Kim, H.J and Christopoulos, C., (2009). "Seismic design procedure and seismic response of post-tensioned self-centering steel frames" *Earthquake Engng Struc. Dyn.*, **38**, 355-376.
- Kim, H.J., Ghaboussi, J. and Elnashai A.S., (2010). "Mechanical and informational modeling of steel beam-to-column connections" *Engineering Structures*, **32**, 449-458.
- López-Barraza A., Ruiz S.E., Bojórquez E., Reyes-Salazar A.,(2012). "Seismic performance of steel frames with pos-tensioned connections", *15 World Conference on Earthquake Engineering*.
- Pirmoz, A. and Danesh, F., (2009). "The seat angle role on moment-rotation response of bolted angle connection" *Electronic of Structural Engineering*, **9**, 73-79.
- MCBC, (2004). "Reglamento de Construcciones del Distrito Federal". (In spanish)
- Reyes-Salazar A. and Haldar, A (2001). "Seismic Response and Energy Dissipation in Partially Restrained and Fully Restrained Steel Frames: an Analytical Study, *Steel and Composite Structures an International Journal*, **1**(4), 459-480.
- Richard, R.M. and Abbott, B.J. (1975). "Versatile elastic-plastic stress-strain formula", *J. Eng. Mech. Div.*, **101**(4), 511-515.
- Ricles, J.M., Sause, R., Garlock, M.M. and Zhao, C. (2001). "Posttensioned seismic-resistant connections for steel frames", *ASCE Journal of Structural Engineering*, **127**(2), 113-121.
- Ricles, J.M., Sause, R., Peng, S.W. and Lu, L.W. (2002). "Experimental evaluation of earthquake resistant posttensioned steel connections", *ASCE Journal of Structural Engineering*, **128**(7), 850-859.

- Ricles, J.M., Sause, R., Lin, Y. C. and Seo, C. Y. (2010). "Self-Centering Moment Connections for Damage-Free Seismic Response of steel MRFs", *2010 structures congress ASCE*, 955-966
- Shen, J., and Astanteh-Asl, A. (1999). "Hysteretic behavior of bolted angle connections." *J. Constr. Steel Res.*, **51**, 201–218.
- Terán-Gilmore A. (1996), "Performance-Based Earthquake-Resistant Design of Framed Buildings Using Energy Concepts". Tesis (PhD in Civil Engineering) University of California, Berkeley.
- Terán-Gilmore, A. (2001). "Consideraciones del uso de la energía plástica en el diseño sísmico", *Revista de ingeniería Sísmica, SMIS*, **65**, 81-110.
- Terán-Gilmore, A. and Jirsa, J.O. (2005). A damage model for practical seismic design that accounts for low cycle fatigue. *Earthquake Spectra*. **21**(3), 803-832.
- Terán-Gilmore, A. and Jirsa, J.O. (2007), "Energy demands for seismic design against low-cycle fatigue", *Earthquake Engineering and Structural Dynamics*, **36**, 383-404.
- Tong G., Lianglong S. and Guodong Z. (2011) "Numerical simulation of the seismic behavior of self-centering steel beam-column connections with bottom flange friction devices" *Earthquake engineering and engineering vibration*, **10**, 229-238.
- Trifunac MD, Brady AG. (1975) "A study of the duration of strong earthquake ground motion", *Bull Seismol Soc Am* ;**65**(3), 581–626.
- Uang C. M. and Bertero, V. V. (1990). "Evaluation of seismic energy in structures", *Earthquake Engineering and Structural Dynamics*, **19**, 77-89.
- Wolski, M., Ricles, J.M. and Sause R. (2009) "Experimental study of self-centering beam-column connection with bottom flange friction device", *ASCE Journal of Structural Engineering*, **135**(5).

## FIGURES AND TABLES

Fig. 1 Schematic structure

Fig. 2 Basic arrangement of a post-tensioned frame connected with bolted angles.

Fig. 3 Monotonic and cyclic response, angle L152x10,  $g_a=100$  mm.

Fig. 4 Connection PT a) Original configuration, b) Deformed configuration

Fig. 5 Comparison of the  $M-\theta r$  curves of Eqs.(1) and (2) with the experimental results.

Fig. 6 Inter-story drift in F10PT under record 1 scaled to  $Sa(T_1)=1.3g$

Fig. 7  $E_H$  in F10PT under record 1 scaled to  $Sa(T_1)=1.3g$

Fig. 8 Median maximum inter-story drift obtained for model F10PT

Fig. 9  $E_H$  dissipated by connections, beams and columns in F10PT for a target median  $\gamma=0.030$

Fig. 10  $E_H$  dissipated in each level of F10PT by columns, beams and connections for a target median  $\gamma = 0.030$

Fig. 11 Distribution of  $F_{EH}$  along the height for different values of  $\gamma$ .

Fig. 12 Comparison of  $F_{EH}$  using Eq. (3) with the result of the numerical analysis for all the models and several values of  $\gamma$ .

Table 1 Ground motion Records

Table 2 Relation between maximum inter-story drift and the seismic intensity

Table 3 Total  $E_H$  dissipated by columns, beams and connections corresponding to various demands of maximum inter-story drift

Table 4  $F_{EH}$  calculated using Eq. (3)

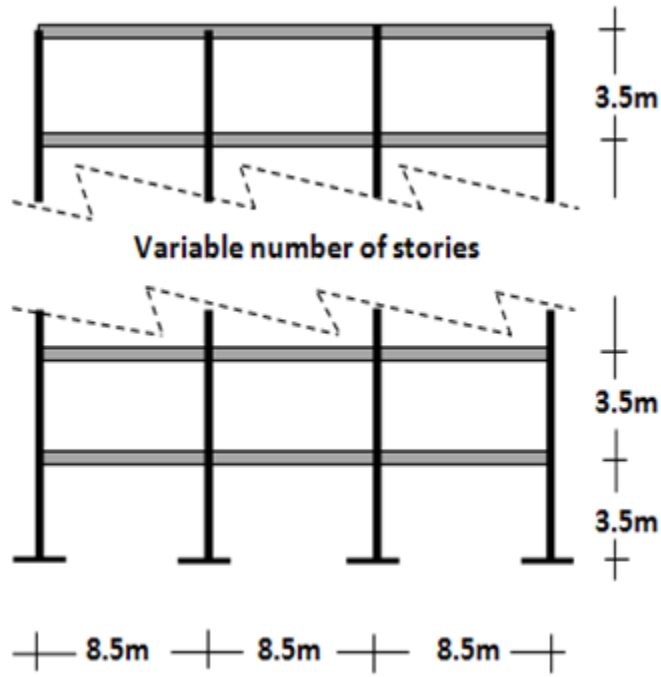


Fig. 1 Schematic structure

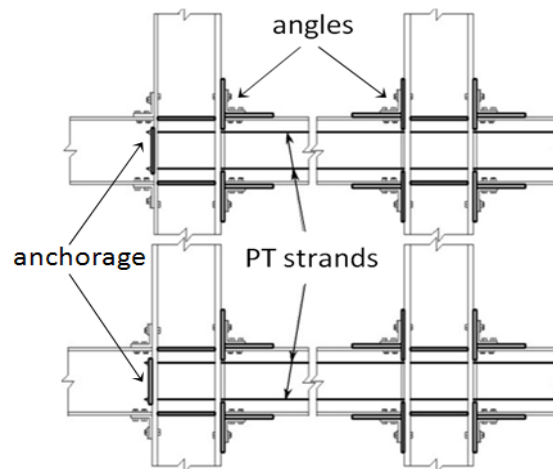


Fig. 2 Basic arrangement of a post-tensioned frame connected with bolted angles.

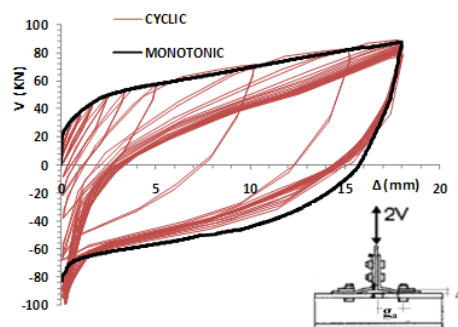


Fig.3 Monotonic and cyclic response, angle L152x10,  $g_a=100$  mm.

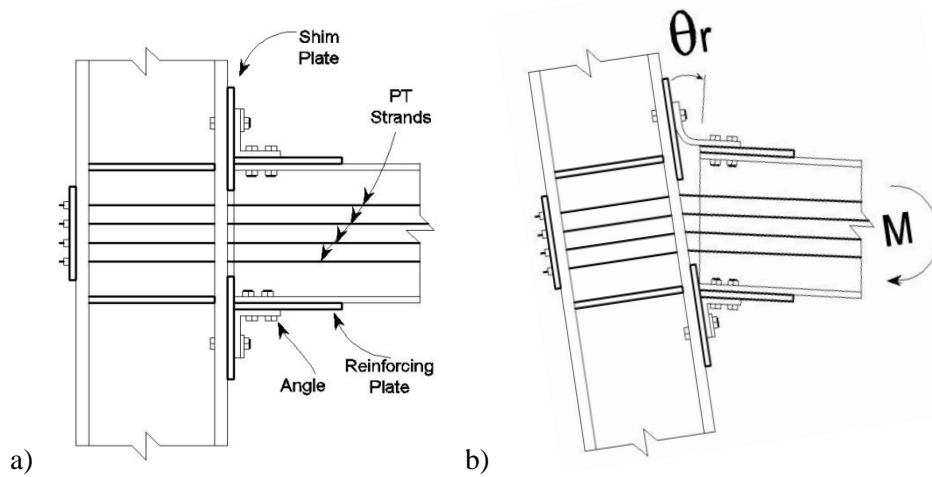
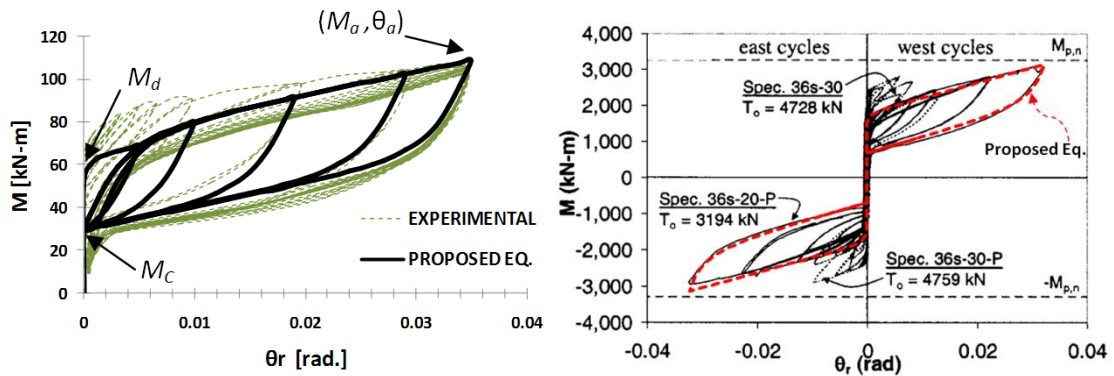


Fig. 4 PT connection a) Original configuration, b) Deformed configuration



a) Proposed equations and experimental results      b) Proposed equations and Garlock results

Fig. 5 Comparison of the  $M-\theta_r$  curves of Eq. (1) and (2) with the experimental results

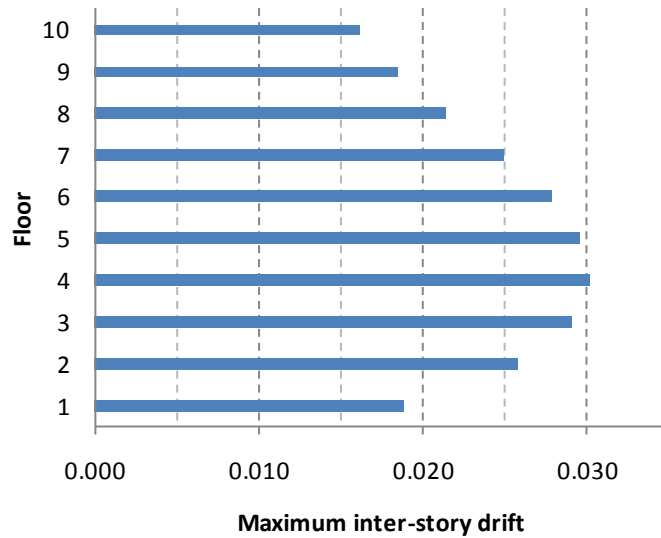
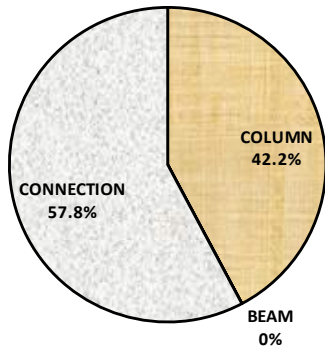
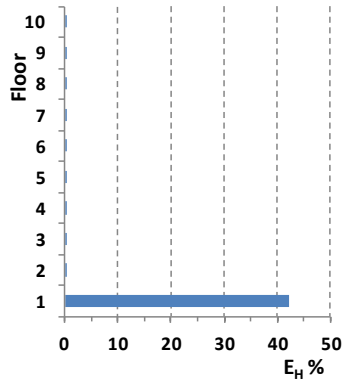


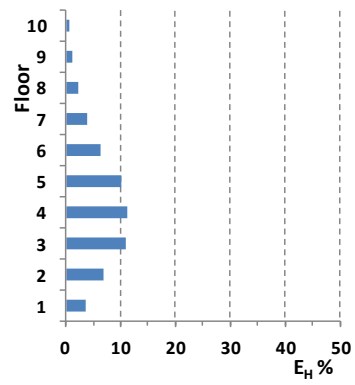
Fig. 6 Inter-story drift in F10PT under record 1 scaled to  $Sa(T_1)=1.3g$



a)  $E_H$  total



b) Distribution in columns



c) Distribution in connections

Fig. 7  $E_H$  in F10PT under record 1 scaled to  $Sa(T_1)=1.3g$

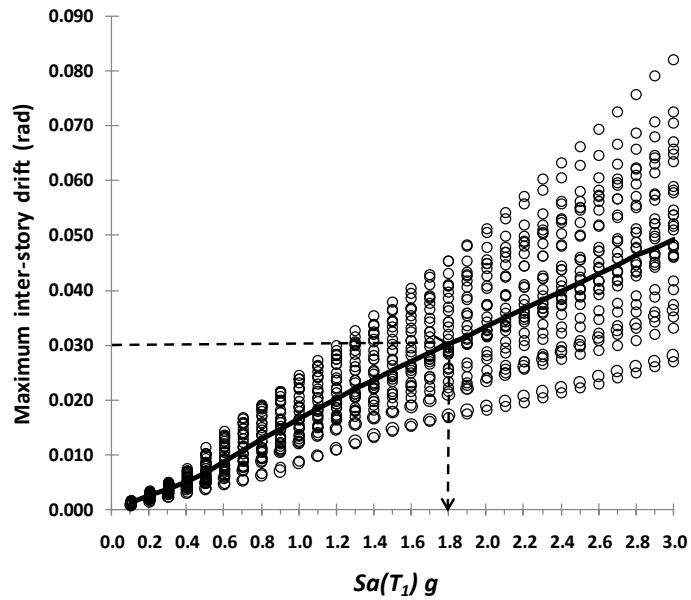


Fig. 8 Median maximum inter-story drift obtained for model F10PT

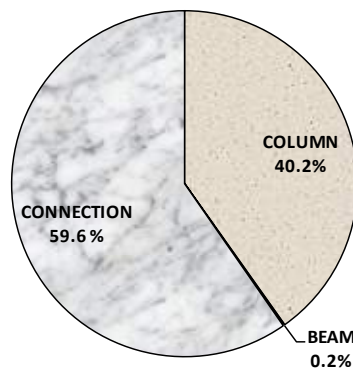


Fig. 9  $E_H$  dissipated by connections, beams and columns in F10PT for a target median  $\gamma=0.030$

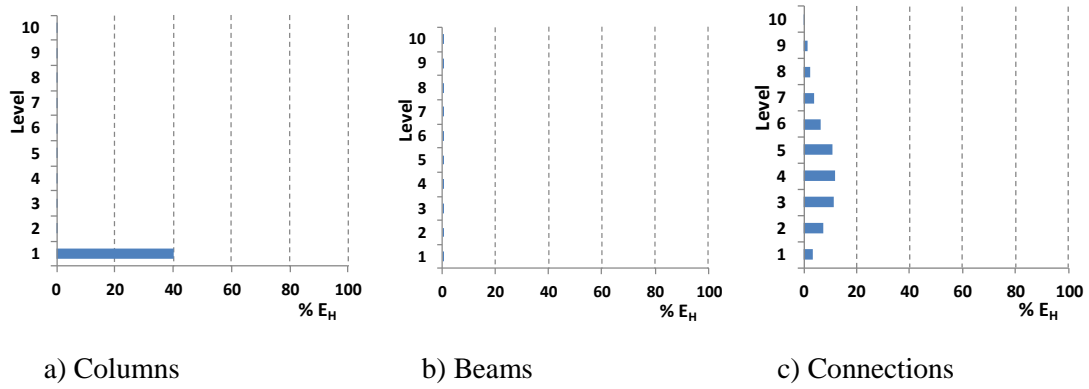


Fig. 10  $E_H$  dissipated in each level of F10PT by columns, beams and connections for a target median  $\gamma = 0.030$

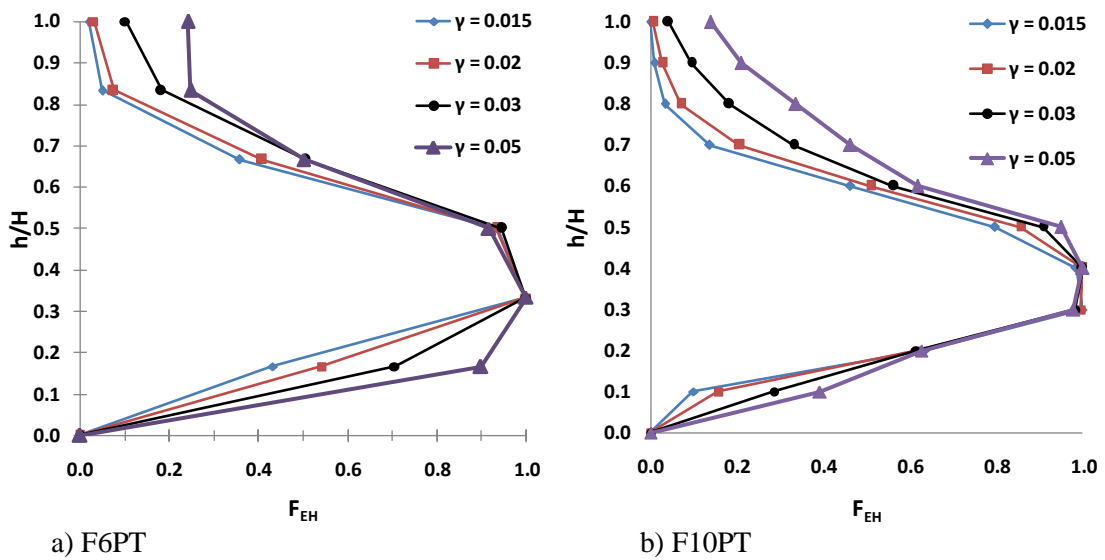


Fig. 11 Distribution of  $F_{EH}$  along the height for different values of  $\gamma$ .

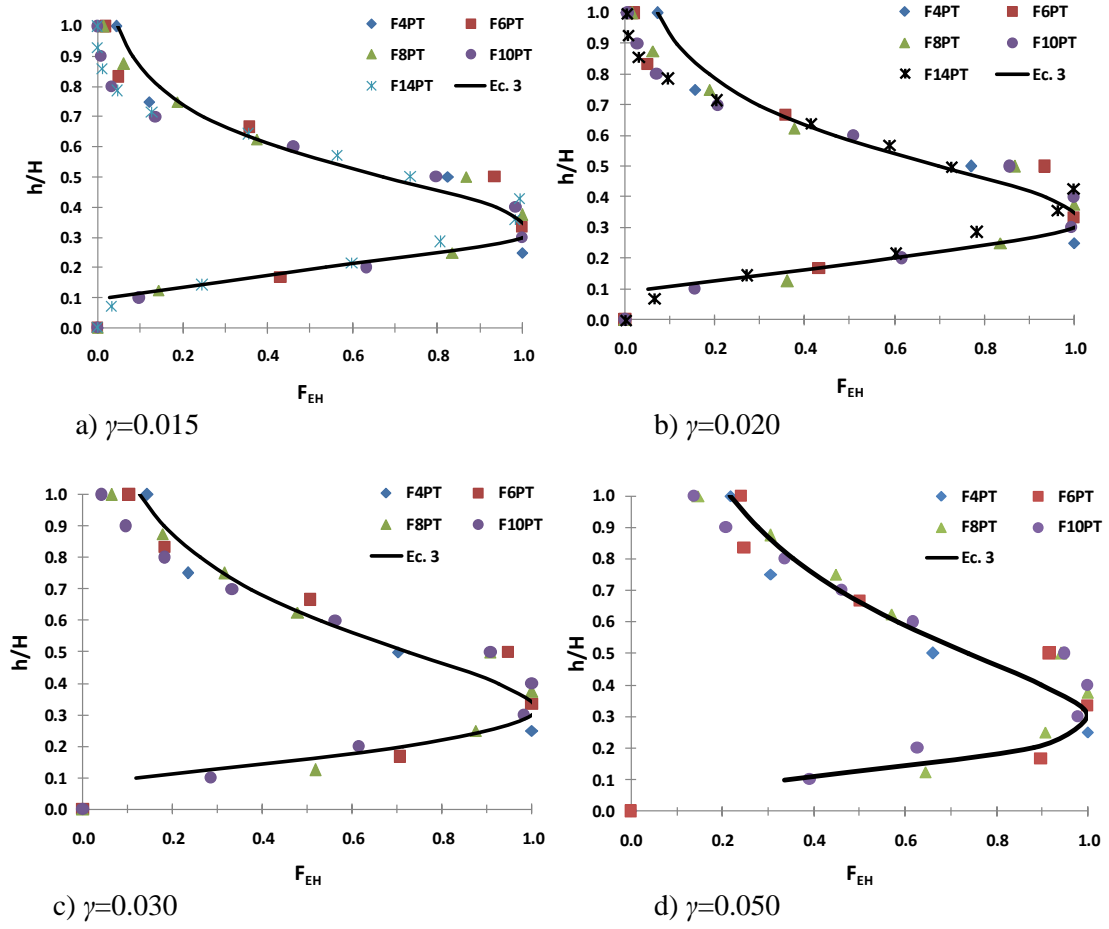


Fig. 12 Comparison of  $F_{EH}$  using Eq. (3) with the result of the numerical analysis for all the models and several values of  $\gamma$ .

Table 1 Ground motion Records

Record	Date	Magnitude	Station	$A_{ms}$ (cm/s <sup>2</sup> )	$V_{ms}$ (cm/s <sup>2</sup> )	Duration (s)
1	19/09/1985	8.1	SCT	178	59.5	164
2	21/09/1985	7.6	Tlahuac deportivo	48.7	14.6	109
3	25/04/1989	6.9	Alameda	45	15.6	93
4	25/04/1989	6.9	Garibaldi	68	21.5	106
5	25/04/1989	6.9	SCT	44.9	12.8	108
6	25/04/1989	6.9	Sector Popular	45.1	15.3	118
7	25/04/1989	6.9	Tlatelolco TL08	52.9	17.3	92
8	25/04/1989	6.9	Tlatelolco TL55	49.5	17.3	84
9	14/09/1995	7.3	Alameda	39.3	12.2	108
10	14/09/1995	7.3	Garibaldi	39.1	10.6	150
11	14/09/1995	7.3	Liconsa	30.1	9.62	130
12	14/09/1995	7.3	Plutarco Elías Calles	33.5	9.37	97
13	14/09/1995	7.3	Sector Popular	34.3	12.5	157
14	14/09/1995	7.3	Tlatelolco TL08	27.5	7.8	125
15	14/09/1995	7.3	Tlatelolco TL55	27.2	7.4	99
16	09/10/1995	7.5	Cibeles	14.4	4.6	105
17	09/10/1995	7.5	CU Juárez	15.8	5.1	125
18	09/10/1995	7.5	Centro urbano Presidente Juárez	15.7	4.8	106
19	09/10/1995	7.5	Córdoba	24.9	8.6	124
20	09/10/1995	7.5	Liverpool	17.6	6.3	126
21	09/10/1995	7.5	Plutarco Elías Calles	19.2	7.9	171
22	09/10/1995	7.5	Sector Popular	13.7	5.3	141
23	09/10/1995	7.5	Valle Gómez	17.9	7.18	79
24	11/01/1997	6.9	CU Juárez	16.2	5.9	77
25	11/01/1997	6.9	Centro urbano Presidente Juárez	16.3	5.5	122
26	11/01/1997	6.9	García Campillo	18.7	6.9	102
27	11/01/1997	6.9	Plutarco Elías Calles	22.2	8.6	115
28	11/01/1997	6.9	Est. # 10 Roma A	21	7.76	111
29	11/01/1997	6.9	Est. # 11 Roma B	20.4	7.1	123
30	11/01/1997	6.9	Tlatelolco TL08	16	7.2	76

Table 2 Relation between maximum inter-story drift and the seismic intensity

$\bar{\gamma}$	$Sa(T_1)$				
	<i>F4PT</i>	<i>F6PT</i>	<i>F8PT</i>	<i>F10PT</i>	<i>F14PT</i>
0.015	0.7g	0.9g	0.8g	0.9g	2.0g
0.020	0.8g	1.0g	1.0g	1.1g	2.7g
0.030	1.0g	1.3g	1.3g	1.8g	*
0.050	1.4g	1.9g	1.9g	3.0g	*

\* Not calculated, because the probability of having values greater than 3g is small.

Table 3 Total  $E_H$  dissipated by columns, beams and connections corresponding to various demands of maximum inter-story drift

Frame	Drift	$E_H$ %		
		Columns	Beams	Connection
F4PT	$\gamma=0.015$	70.9	0.4	28.7
	$\gamma=0.020$	69.0	3.2	27.8
	$\gamma=0.030$	64.6	8.2	27.2
	$\gamma=0.050$	59.6	13.2	27.3
F6PT	$\gamma=0.015$	53.4	2.1	44.4
	$\gamma=0.020$	54.4	3.2	42.4
	$\gamma=0.030$	53.9	6.3	39.8
	$\gamma=0.050$	50.9	13.4	35.6
F8PT	$\gamma=0.015$	36.7	0.3	63.0
	$\gamma=0.020$	42.9	0.7	56.4
	$\gamma=0.030$	48.0	2.8	49.2
	$\gamma=0.050$	48.2	8.2	45.6
F10PT	$\gamma=0.015$	19.0	0.4	80.6
	$\gamma=0.020$	27.7	0.3	72.0
	$\gamma=0.030$	40.2	0.2	59.6
	$\gamma=0.050$	45.3	2.8	52
F14PT	$\gamma=0.015$	1.0	0.7	98.2
	$\gamma=0.020$	6.6	0.5	92.9
	$\gamma=0.030$	*	*	*
	$\gamma=0.050$	*	*	*

Table 4  $F_{EH}$  calculated using Eq. (3)

h/H	$\gamma = 0.015$	$\gamma = 0.02$	$\gamma = 0.03$	$\gamma = 0.05$
0.1	0.024	0.049	0.135	0.416
0.2	0.517	0.600	0.739	0.939
0.3	1.000	1.000	1.000	1.000
0.4	0.957	0.938	0.909	0.869
0.5	0.691	0.700	0.707	0.702
0.6	0.438	0.470	0.513	0.550
0.7	0.261	0.301	0.361	0.427
0.8	0.151	0.188	0.251	0.331
0.9	0.086	0.117	0.174	0.257
1	0.049	0.072	0.121	0.200